

# A new test of local Lorentz invariance using $^{21}\text{Ne}$ -Rb-K comagnetometer

M. Smiciklas, J. M. Brown, L.W. Cheuk, and M. V. Romalis  
*Department of Physics, Princeton University, Princeton, New Jersey 08544*

We develop a new comagnetometer using  $^{21}\text{Ne}$  atoms with nuclear spin  $I = 3/2$  and Rb atoms polarized by spin-exchange with K atoms to search for tensor interactions that violate local Lorentz invariance. We frequently reverse orientation of the experiment and search for signals at the first and second harmonics of the sidereal frequency. We constrain 4 of the 5 spatial Lorentz-violating coefficients  $c_{jk}^n$  that parameterize anisotropy of the maximum attainable velocity of a neutron at a level of  $10^{-29}$ , improving previous limits by 2 to 4 orders of magnitude and placing the most stringent constrain on deviations from local Lorentz invariance.

PACS numbers: 11.30.Cp, 21.30.Cb, 32.30.Dx

The Michelson-Morley experiment and its successors have established that the speed of light is isotropic to a part in  $10^{17}$  [1, 2]. Similarly, possible anisotropy in the maximum attainable velocity (MAV) for a massive particle [3] has been constrained by Hughes and Drever NMR experiments [4, 5] and their successors to a part in  $10^{27}$  [6]. These experiments form the basis for the principle of local Lorentz invariance (LLI). Together with the weak equivalence principle and the position invariance principle, they constitute the Einstein equivalence principle that is the basis of general relativity [7]. Measurements of tensor NMR energy shifts [8, 9] are particularly sensitive to variation in MAV due to a finite kinetic energy of valence nucleons. They place the most stringent limits on violation of LLI within the  $TH\epsilon\mu$  formalism [10] describing deviations from the Einstein Equivalence Principle as well as within more general Standard Model Extension (SME) [11]. They compare favorably even to the limits on variation in MAV from ultra-high energy cosmic rays and other astrophysical phenomena [12–14]. It can be argued that Lorentz invariance is likely to be broken at some level by the effects of quantum gravity, which contains a dimensionfull Planck scale that is not Lorentz-invariant. Popular ideas for quantum gravity theories, such as recently proposed Hořava-Lifshitz model [15], explicitly violate Lorentz symmetry. CPT-even tensor Lorentz-violating effects, such as variation in MAV, are particularly interesting to explore because they can arise from purely kinematic violation of Lorentz invariance, do not require explicit particle spin coupling at the fundamental level, and do not suffer from fine-tuning problems associated with CPT-odd Lorentz-violating vector spin interactions [16, 17].

Here we describe a new comagnetometer that is sensitive to anisotropy in neutron MAV at  $10^{-29}$  level. The idea of the experiment is based on the K- $^3\text{He}$  comagnetometer, previously used to constrain Lorentz-violating vector spin interactions [18]. The  $^3\text{He}$  ( $I = 1/2$ ) is replaced by  $^{21}\text{Ne}$  ( $I = 3/2$ ) to allow measurements of tensor anisotropy. In addition, since the gyromagnetic ratio of  $^{21}\text{Ne}$  is about an order of magnitude smaller than that of  $^3\text{He}$ , the comagnetometer has an order of magnitude better energy resolution for the same level of magnetic field

sensitivity. The electric quadrupole interactions of  $^{21}\text{Ne}$  cause several problems. In order to overcome a faster nuclear spin relaxation in  $^{21}\text{Ne}$  relative to  $^3\text{He}$ , we replace K with Rb atoms, which have a larger spin-exchange cross-section with  $^{21}\text{Ne}$  [19]. We also increase the alkali density by an order of magnitude and rely on hybrid optical pumping [20], using spin-exchange with optically-pumped K to polarize the Rb atoms while avoiding strong absorption of pumping light by the optically dense Rb vapor.

The experiment is placed on a rotary platform and its orientation can be frequently reversed to introduce a modulation of the Lorentz-violating signal (Fig. 1). Among lab-fixed backgrounds, only the gyroscopic signal due to the Earth’s rotation cannot be easily suppressed, and we rely on sidereal and semi-sidereal oscillations expected for Lorentz-violating effects to extract anisotropic signals of an extra-solar origin. We measure the  $^{21}\text{Ne}$  NMR frequency with a sensitivity of about 0.5 nHz and, within the Schmidt model for the  $^{21}\text{Ne}$  nucleus, constrain 4 of the 5 spatial components of the symmetric traceless SME tensor  $c_{jk}^n$  for neutrons at a level of a few parts in  $10^{29}$ . This sensitivity exceeds all other limits on the  $c_{\mu\nu}$  coefficients in the matter sector [21] as well as the recent limit on the neutrino  $c_{0j}$  coefficient at a level of  $10^{-27}$  [22] and limits on  $c_{00}$  at a level of  $10^{-23}$  from analysis of ultra-high energy cosmic rays [14, 23].

The operating principles of the comagnetometer are similar to that described in [18, 24, 25]. The atoms are contained in a 1.4 cm diameter spherical cell made from aluminosilicate glass that is filled with Ne (enriched to 95% of  $^{21}\text{Ne}$ ) at a density of  $2.03 \pm 0.05$  amagat as determined from pressure broadening of Rb D1 line [26], 30 Torr of  $\text{N}_2$  for quenching, and a mixture of  $^{87}\text{Rb}$  and K alkali metals. The cell is heated to about  $200^\circ\text{C}$  by AC currents at 170 kHz in a twisted pair wire heater. The density of Rb at the operating temperature is measured to be  $5.5 \times 10^{14} \text{ cm}^{-3}$ , while the density of K is about  $2 \times 10^{12} \text{ cm}^{-3}$ . K atoms are optically pumped by 650 mW of circularly-polarized light from an amplified distributed Bragg reflector diode laser at 770 nm. Rb atoms are polarized to 40% by Rb-K spin exchange collisions, while  $^{21}\text{Ne}$  atoms are polarized to 15-17% by

spin-exchange with Rb. The comagnetometer signal is measured by monitoring optical rotation of a 10 mW linearly polarized probe beam that is generated by a distributed feedback diode laser near the 795 nm Rb D1 transition. The comagnetometer cell is placed inside magnetic shields consisting of 3 layers of  $\mu$ -metal and an inner ferrite shield with an overall shielding factor of  $10^8$ . Coils inside the magnetic shields are used to cancel residual magnetic fields and create a compensation field  $B_z = -8\pi\kappa_0(M_{Rb} + M_{Ne})/3$ , where  $M_{Rb}$  and  $M_{Ne}$  are the magnetizations of electron and nuclear spins, and  $\kappa_0 = 34 \pm 3$  is the contact spin-exchange enhancement factor for Rb- $^{21}\text{Ne}$  [19, 27]. At this compensation field, the comagnetometer signal is insensitive to slowly-changing magnetic fields in all three directions while retaining sensitivity to anomalous interactions that couple, for example, only to nuclear or to electron spins. Changes in the sensitivity of the comagnetometer are periodically monitored by application of an oscillating  $B_x$  field [18]. The optical setup is contained in a bell jar evacuated to 2 Torr to eliminate noise from air currents. The apparatus and all electronics are mounted on a rotation platform and can be fully rotated around the vertical axis in several seconds. To compensate for a shift in the sensitive direction of the co-magnetometer due to an AC Stark shift caused by the 770 nm pump laser at the 780 nm Rb D2 line, we rotate the apparatus by  $13^\circ$  from the nominal  $\hat{y}$  direction toward  $\hat{x}$ .

A representative sample of the comagnetometer signal during normal data collection is shown in Fig. 2. The orientation of the platform is reversed by  $180^\circ$  every 22 sec. We usually collect data in the North-South (NS) orientations of the sensitive axis, which gives a maximum gyroscopic signal due to the Earth's rotation and in the East-West (EW) orientations, which gives nominally zero gyroscopic signal. After each mechanical rotation a background measurement of optical rotation is performed with  $B_z$  field detuned by  $0.33 \mu\text{T}$  to suppress the spin response. Data collection is periodically paused (300 to 400

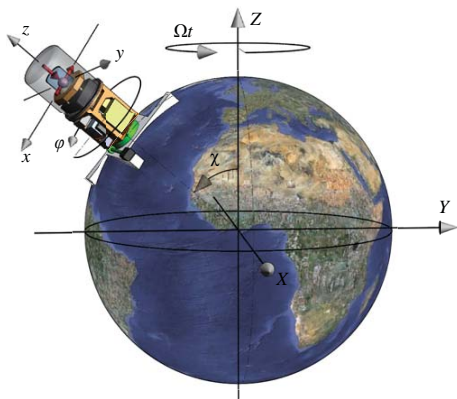


FIG. 1: The experimental apparatus is rotated around the local vertical.  $^{21}\text{Ne}$  spins are polarized down along  $-\hat{z}$  and the probe beam is directed horizontally along  $-\hat{x}$

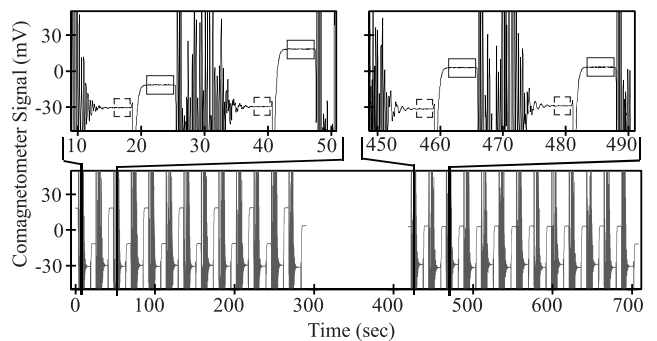


FIG. 2: Magnetometer signal as a function of time. During the first 300 seconds the sensitive axis is alternated between North and South directions. After the transient from rotation decays, the background optical rotation is measured (dashed box). Then  $B_z$  field is set to the compensation point and actual signal is measured (solid box). Rotations are paused after 13 reversals for calibration. In the following sequence the sensitive axis is alternated between East and West.

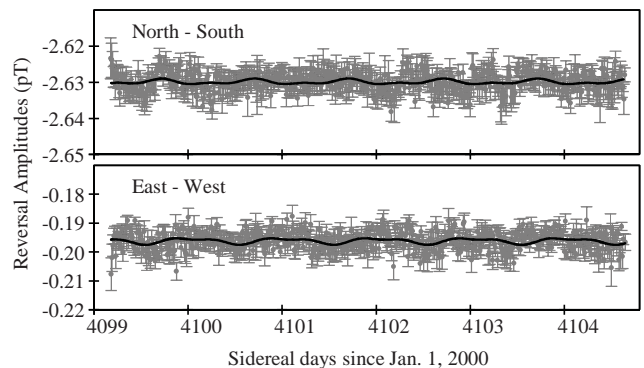


FIG. 3: Long-term measurements of the N-S and E-W modulation amplitudes with a fit including first and second harmonics of the sidereal frequency.

sec in Fig. 2) to adjust the compensation value of  $B_z$  field and measure the sensitivity of the magnetometer. Fig. 3 shows an example of long-term measurements of the amplitudes of NS and EW modulations after subtraction of optical rotation background. We make a 10% correction to the calibration of the comagnetometer based on the size of the gyroscopic signal due to Earth's rotation  $B_{\text{eff}} = \Omega_{\oplus} I \sin \chi / \mu_{Ne} = 2.63 \text{ pT}$  in the NS data. Slow drifts in the NS and EW signals are caused by changes in various experimental parameters. We perform a correlation analysis between the comagnetometer signal and several measured temperatures, laser beam position monitors, tilts,  $^{21}\text{Ne}$  polarization, and other parameters. We find a small but finite correlation of the signal with oven temperature, room temperature, and  $^{21}\text{Ne}$  polarization. These correlations are removed from the data while ensuring that diurnal changes in the temperature do not accidentally cancel a real sidereal signal in the data.

We interpret these measurements within a sub-set of

the SME, adding  $c_{\mu\nu}$  coefficients to the standard relativistic Lagrangian of a fermion,

$$\mathcal{L} = \frac{1}{2} i \bar{\psi} (\gamma_\nu + c_{\mu\nu} \gamma^\mu) \overleftrightarrow{\partial}^\nu \psi - \bar{\psi} m \psi. \quad (1)$$

In the non-relativistic limit, this leads to an anisotropic energy shift for a particle with spatial components of momentum  $p_j$ , which can be written as a product of spherical tensor operators of rank 2,  $\mathcal{C}_n^2$  and  $\mathcal{P}_n^2$ , formed from Cartesian components of  $c_{jk}$  and  $p_j p_k$  respectively,

$$H = -c_{jk} p_j p_k / m = -(-1)^n \mathcal{C}_n^2 \mathcal{P}_{-n}^2 / m. \quad (2)$$

Using the Wigner-Eckart theorem, we evaluate the matrix elements of  $\mathcal{P}_n^2$  in terms of  $\mathcal{I}_n^2$ , the rank-2 spherical tensor formed from components of nuclear spin  $I$ ,

$$\langle I, m | \mathcal{P}_n^2 | I, m' \rangle = \frac{\langle I, m | \mathcal{I}_n^2 | I, m' \rangle \langle I, I | \mathcal{P}_0^2 | I, I \rangle}{\langle I, I | \mathcal{I}_0^2 | I, I \rangle}. \quad (3)$$

In the coordinate system defined in Fig. 1, the comagnetometer is sensitive to first order to the energy of the  $^{21}\text{Ne}$  nuclear magnetic moment  $\mu_{Ne}$  interacting with the magnetic field in the  $\hat{y}$  direction [18],

$$H_B = -\mu_{Ne} I_y B_y / |I|. \quad (4)$$

Among tensor nuclear spin operators, the comagnetometer is sensitive to first order to the operator

$$H_Q = -Q(I_y I_z + I_z I_y) / 2 = -iQ(\mathcal{I}_1^2 + \mathcal{I}_{-1}^2) / 2, \quad (5)$$

since  $I_z$  has a finite expectation value due to longitudinal nuclear polarization of  $^{21}\text{Ne}$ . This gives sensitivity to the  $i(\mathcal{C}_1^2 + \mathcal{C}_{-1}^2)$  combination of the spherical tensor components of the  $c_{jk}$  coefficients in the frame of the experiment. Transforming into the geocentric equatorial coordinate system, we obtain expressions for the NS and EW signals as a function of time,

$$\begin{aligned} S_{NS} &= -c'_Y \cos 2\chi \cos \Omega_\oplus t - c'_X \cos 2\chi \sin \Omega_\oplus t - \\ &\quad (c'_Z \sin 2\chi \cos 2\Omega_\oplus t + c'_- \sin 2\chi \cos 2\Omega_\oplus t) / 2 \\ S_{EW} &= c'_X \cos \chi \cos \Omega_\oplus t - c'_Y \cos \chi \sin \Omega_\oplus t + \\ &\quad c'_Z \sin \chi \cos 2\Omega_\oplus t - c'_- \sin \chi \sin 2\Omega_\oplus t, \end{aligned} \quad (6)$$

where the  $c$  parameters are defined in Table I [21],  $\chi = 49.6^\circ$  in Princeton, and  $t$  is the local sidereal time. Primes on  $c$  coefficients indicate that they are measured experimentally in magnetic field units. The signal contains both first and second harmonics of the Earth rotation rate  $\Omega_\oplus$ . Each component of the  $c$  tensor can be determined independently from NS and EW signals, although sensitivity to the first harmonic in the NS data is suppressed because  $\cos 2\chi = -0.16$ . Vector Lorentz-violating interactions, such as the  $b_\mu$  coefficient, can contribute to the first harmonic signal, however within the Schmidt nuclear model for  $^{21}\text{Ne}$  with a valence neutron such an interaction has already been excluded with sufficient precision by previous experiments with  $^3\text{He}$  [18]

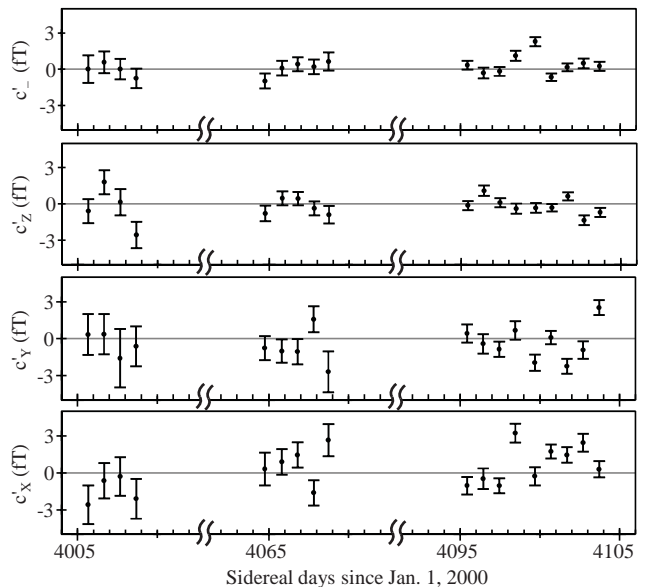


FIG. 4: Daily fits for the  $c$  coefficients defined in Eq. (6). The final statistical uncertainty is increased to account for reduced  $\chi^2 = 2$  to 4.

and electrons [28]. The results of the daily fits for the  $c$  coefficients are shown in Fig. 4 for our data spanning a period of 3 months and the final results are summarized in Table I. The systematic uncertainty is determined by the scatter of several analysis procedures, including fits of data without removal of long-term correlations and varying data cuts.

To convert our measurements from magnetic field units, we need an estimate of the nuclear operator  $\langle I, I | \mathcal{P}_0^2 | I, I \rangle = \langle I, I | 2p_z^2 - p_x^2 - p_y^2 | I, I \rangle / \sqrt{6}$ . Within the Schmidt model,  $^{21}\text{Ne}$  has a valence neutron in the  $d_{3/2}$  state. This gives  $\langle I, I | \mathcal{P}_0^2 | I, I \rangle = -\sqrt{2/3} \langle p^2 \rangle / 5 = -\sqrt{8/3} m E_k / 5$  and we take the kinetic energy of the valence nucleon  $E_k \sim 5$  MeV [6].  $^{21}\text{Ne}$  is better described by a collective wavefunction within the  $sd$  shell model, and it should be possible to calculate the nuclear operator more precisely [29].

To evaluate the relative sensitivity of the comagnetometer to  $H_B$  and  $H_Q$ , we model the equilibrium spin density matrix of  $^{21}\text{Ne}$ . Two processes dominate the spin evolution of  $^{21}\text{Ne}$ , binary spin-exchange collisions with Rb [30] and spin-relaxation due to the interaction of its nuclear electric quadrupole moment with electric field gradients during binary atomic collisions [31]. At low Rb density, we measured  $^{21}\text{Ne}$  spin relaxation time constant  $T_Q = 87 \pm 4$  min, close to the relaxation rate of  $103 \pm 6$  min that is predicted for our  $^{21}\text{Ne}$  density from previous measurements of the  $^{21}\text{Ne}$  nuclear quadrupole relaxation rate [19]. At normal operating temperature, the  $^{21}\text{Ne}$  spin time constant was equal to  $63 \pm 2$  min, implying an additional Rb- $^{21}\text{Ne}$  spin-exchange time constant  $T_{ex} = 230 \pm 40$  min. This is reasonably consistent with Rb- $^{21}\text{Ne}$  spin-exchange time constant of  $370 \pm 70$

	North-South (fT)	East-West (fT)	Combined (fT)	Scaled
$c_X = c_{YZ}^n + c_{ZY}^n$	$-0.9 \pm 1.8 \pm 2.3$	$0.75 \pm 0.39 \pm 0.50$	$0.67 \pm 0.62$	$(4.8 \pm 4.4) \times 10^{-29}$
$c_Y = c_{XZ}^n + c_{ZX}^n$	$0.7 \pm 1.3 \pm 2.5$	$-0.42 \pm 0.36 \pm 0.33$	$-0.39 \pm 0.48$	$-(2.8 \pm 3.4) \times 10^{-29}$
$c_Z = c_{XY}^n + c_{YX}^n$	$0.01 \pm 0.34 \pm 0.27$	$-0.23 \pm 0.19 \pm 0.13$	$-0.17 \pm 0.20$	$-(1.2 \pm 1.4) \times 10^{-29}$
$c_- = c_{XX}^n - c_{YY}^n$	$0.65 \pm 0.34 \pm 0.32$	$0.04 \pm 0.19 \pm 0.20$	$0.20 \pm 0.24$	$(1.4 \pm 1.7) \times 10^{-29}$

TABLE I: Results for the neutron  $c_{jk}^n$  coefficients measured in  $^{21}\text{Ne}$ .

min calculated from a previously measured Rb- $^{21}\text{Ne}$  spin-exchange rate constant [19]. The equilibrium  $^{21}\text{Ne}$  polarization of 17% is also consistent with measured Rb polarization and spin-exchange and relaxation rates. In the density matrix model for the comagnetometer, we find the ratio of the signals produced by  $H_B$  and  $H_Q$ ,

$$\frac{S(Q)}{S(B_y)} = \frac{Q \langle I_z \rangle}{2\mu_{Ne} B_y / I} f(T_{ex}/T_Q) \quad (7)$$

where the function  $f(T_{ex}/T_Q)$  ranges from  $f(0) = 1$  to  $f(\infty) = 3/2$  as the population distribution among the four spin states of  $^{21}\text{Ne}$  changes depending on the nature of the dominant spin relaxation mechanism. For our operating parameters  $f(2.6 \pm 0.4) = 1.27 \pm 0.03$ . The conversion factor to dimensionless  $c$  coefficients parameterizing variations in the neutron MAV is

$$c = -c' \frac{10\mu_n}{3P_{Ne} f E_k} = 7.1 \times 10^{-29} \quad (8)$$

and our results for the neutron  $c_{jk}^n$  are given in the last column of Table I.

Our limits are 2 to 4 orders of magnitude more stringent than previous limits set with similar experiments using  $^7\text{Be}$  [32],  $^{201}\text{Hg}$  [8], and  $^{21}\text{Ne}$  [9] spins. They are also 4 orders of magnitude more stringent than limits on

similar proton  $c$  coefficients set using  $^{133}\text{Cs}$  atomic fountain clock [33] and many orders of magnitude more sensitive than limits for electron  $c$  coefficients [21]. Among astrophysical tests, the most stringent limits have been set on  $c_{0j}$  for neutrinos by Icecube at  $10^{-27}$  [22] and on  $c_{00}$  for protons at  $10^{-23}$  from analysis of the spectrum of ultra-high energy cosmic rays [14, 23]. Our measurements of the spatial components  $c_{ij}$  are comparable to these results for  $c_{00}$  and  $c_{0j}$  if we assume that Lorentz violation is manifested by a difference between space and time in a preferred frame of the Cosmic Microwave Background, which moves relative to the Earth with a velocity of  $10^{-3}c$  in an approximately equatorial direction.

This measurement represents the first experimental result using the  $^{21}\text{Ne}$ -Rb-K comagnetometer. Our frequency resolution is similar to the previous K- $^3\text{He}$  Lorentz-violation experiment [18] with a factor of 8 shorter integration time and without full optimization of the apparatus. The shot-noise sensitivity of the comagnetometer is already more than an order of magnitude better than the best results obtained with K- $^3\text{He}$  [34], allowing for further improvements in both vector and tensor Lorentz invariance tests as well as other precision measurements by several orders of magnitude. This work was supported by NSF Grant No. PHY-0969862.

- 
- [1] Ch. Eisele, A. Yu. Nevsky, and S. Schiller, Phys. Rev. Lett. **103**, 090401 (2009).  
[2] S. Herrmann, A. Senger, K. Möhle, M. Nagel, E. V. Kovalchuk, and A. Peters, Phys. Rev. D **80**, 105011 (2009).  
[3] S. Coleman and S. L. Glashow, Phys. Rev. D **59**, 116008 (1999).  
[4] V. W. Hughes, H. G. Robinson, and V. Beltran-Lopez, Phys. Rev. Lett. **4**, 342 (1960).  
[5] R. W. P. Drever, Phil. Magazine, **6** 683 (1961).  
[6] V. A. Kostelecký and C. D. Lane, Phys. Rev. D **60**, 116010 (1999).  
[7] C.M. Will, Living Rev. Rel. **9**, 3 (2006).  
[8] S. K. Lamoreaux, J. P. Jacobs, B. R. Heckel, F. J. Raab, and E. N. Fortson, Phys. Rev. Lett. **57**, 3125 (1986).  
[9] T. E. Chupp *et al.*, Phys. Rev. Lett. **63**, 1541 (1989).  
[10] A.P. Lightman and D.L. Lee, Phys. Rev. D, **8**, 364, (1973).  
[11] D. Colladay and V. A. Kostelecký, Phys. Rev. D **58**, 116002 (1998).  
[12] B. Altschul, Phys. Rev. Lett. **96**, 201101 (2006).  
[13] B. Altschul, Phys. Rev. D **78**, 085018 (2008).  
[14] F. W. Stecker and S. T. Scully, New J. Phys. **11**, 085003 (2009).  
[15] P. Hořava, Phys. Rev. D **79**, 084008 (2009).  
[16] D. Mattingly, Proc. of Sci. (QG-Ph) 026, (2008).  
[17] P. A. Bolokhov, S. Groot Nibbelink, and M. Pospelov, Phys. Rev. D **72**, 015013 (2005).  
[18] J. M. Brown, S. J. Smullin, T. W. Kornack, and M. V. Romalis, Phys. Rev. Lett. **105**, 151604 (2010).  
[19] R. K. Ghosh and M. V. Romalis, Phys. Rev. A **81**, 043415 (2010).  
[20] M. V. Romalis, Phys. Rev. Lett. **105**, 243001 (2010).  
[21] V. A. Kostelecký, N. Russell, Rev. Mod. Phys. **83**, 11 (2011).  
[22] R. Abbasi *et al.*, Phys. Rev. D **82**, 112003 (2010).  
[23] X.-J. Bi, Z. Cao, Y. Li, and Q. Yuan, Phys. Rev. D **79**, 083015 (2009).  
[24] T. W. Kornack, R. K. Ghosh and M. V. Romalis, Phys.

- Rev. Lett. **95**, 230801 (2005).
- [25] T.W. Kornack, PhD Dissertation, Princeton University (2005).
- [26] M. D. Rotondaro and G. P. Perram, J. Quan. Spec. Rad. Tran. **57**, 497 (1997).
- [27] S. R. Schaefer, G. D. Cates, T.-R. Chien, D. Gonatas, W. Happer, and T. G. Walker, Phys. Rev. A **39**, 5613 (1989).
- [28] B. R. Heckel *et al.* Phys. Rev. D **78**, 092006 (2008).
- [29] W. Geithner *et al.*, Phys. Rev. C **71**, 064319 (2005).
- [30] W. Happer *et al.*, Phys. Rev. A **29**, 3092 (1984).
- [31] C. Cohen-Tannoudji, J. de Phys. **24**, 653 (1963).
- [32] J. D. Prestage, J. J. Bollinger, Wayne M. Itano, and D. J. Wineland, Phys. Rev. Lett. **54**, 2387 (1985).
- [33] P. Wolf, F. Chapelet, S. Bize, and A. Clairon, Phys. Rev. Lett. **96**, 060801 (2006).
- [34] G. Vasilakis, J. M. Brown, T. W. Kornack, and M. V. Romalis, Phys. Rev. Lett. **103**, 261801 (2009).